

# Aggregation of Colloidal Particles with a Finite Interparticle Attraction Energy

Wan Y. Shih,<sup>1</sup> Jun Liu,<sup>1</sup> Wei-Heng Shih,<sup>1</sup> and Ilhan A. Aksay<sup>1</sup>

*Received July 19, 1990; final October 30, 1990*

---

Aggregation of colloidal particles with a finite attraction energy was investigated with computer simulations and with gold particles coated with a surfactant. Computer simulations were carried out with the Shih-Aksay-Kikuchi (SAK) model, which incorporates a finite nearest-neighbor attraction energy  $-E$  into the diffusion-limited-cluster-aggregation (DLCA) model. Both the computer simulations and the experiments showed that (i) with a finite interparticle attraction energy, aggregates can still remain fractal, and (ii) the fractal dimension remains unchanged at large interparticle attraction energies and increases when the interparticle attraction energy is smaller than  $4k_B T$ , where  $T$  is the temperature and  $k_B$  is the Boltzmann constant. The agreement between the simulations and the experimental results suggests that the reversible aggregation process in a colloidal system can be represented by the SAK model.

---

**KEY WORDS:** Aggregation; colloid.

## 1. INTRODUCTION

Colloidal aggregates have attracted much research interest since it was shown that the concept of a fractal dimension  $D$  can be used to characterize the structure of a disordered system, such as a random aggregate that is formed under nonequilibrium conditions.<sup>(1)</sup> However, under most circumstances, only certain values of the fractal dimension have been found with small gold, silica, and polystyrene particles (size  $\leq 0.1 \mu\text{m}$ ):  $D = 1.75$  for fast aggregation<sup>(2,4)</sup> and  $D = 2.02\text{--}2.12$  for slow aggregation.<sup>(5,7)</sup> Occasionally, the  $D = 1.75$  aggregates may at a later time restructure to higher fractal dimensions,  $D = 2.08\text{--}2.1$  (ref. 3) and  $D = 2.4$  (ref. 4). Computer

---

Department of Materials Science and Engineering, and Advanced Materials Technology Center, Washington Technology Centers, University of Washington, Seattle, Washington 98195.

simulations of the diffusion-limited-cluster-aggregation model (DLCA)<sup>(8,9)</sup> yield  $D = 1.78$  in three dimensions (3D) and seem to represent fast aggregation in the colloidal systems. The reaction-limited-cluster-aggregation model (RLCA)<sup>(10)</sup> is a modification of the DLCA model with a sticking probability  $p$ . Computer simulations of the RLCA model with  $p$  approaching zero, which yield  $D = 2.0$  in three dimensions, seem to be coincident with the result of slow aggregation; however, the RLCA model cannot account for the restructuring of the aggregates. Both the DLCA and RLCA are irreversible aggregation models.

In order to simulate the reversible aggregation process of colloidal particles, modifications to the DLCA model have been considered, since the DLCA model seems to represent colloidal aggregation under irreversible conditions. Kolb<sup>(11)</sup> has modified the DLCA model with random bond breaking, which yields  $D = 1.57 \pm 0.06$  in two dimensions (2D) and  $D = 2.03 \pm 0.05$  in 3D at dynamic equilibrium. Although the Kolb model<sup>(11)</sup> seems to be able to explain the restructuring of silica aggregates,<sup>(3)</sup> it cannot explain the fractal dimension  $D = 2.4$  obtained for gold aggregates<sup>(4)</sup> at a later time.

Meanwhile, various fractal dimensions have been observed experimentally with larger polystyrene particles in 2D (size  $> 1 \mu\text{m}$ ).<sup>(12)</sup> Skjeltorp has shown that aggregates form with  $D = 1.7$ – $2.0$  in fairly concentrated suspensions as a result of changing the particle concentration and/or the salt concentration. Skjeltorp's minimum fractal dimension  $D = 1.7$  in 2D is more consistent with the computer simulations of the diffusion-limited-aggregation model (DLA).<sup>(4)</sup> While Skjeltorp has been able to obtain a band of values for  $D$  and to correlate the fractal dimension with the growth rate of the aggregates, he has not addressed the correlation of the change in the fractal dimension with either the particle concentration or the salt concentration, both of which can change the interparticle interaction in colloidal systems.<sup>(13)</sup>

In this paper, we will review the investigations concerning the effect of the interparticle interaction, especially a finite interparticle attraction energy, on the aggregation of colloidal particles both experimentally and with computer simulations. The computer simulations were done by Shih, Aksay, and Kikuchi (SAK)<sup>(14)</sup> by modifying the DLCA model with a finite interparticle attraction energy  $-E$ . Although the Kolb model and the SAK model are both reversible aggregation models, the bond-breaking processes are very different in the two models. In the Kolb model, the breaking unit is a bond which breaks randomly and independently with a probability  $1/\tau$  per unit time, whereas in the SAK model, bond breaking is not random; the breaking unit is a particle which breaks its bond with its neighbors according to the Boltzmann factor  $(1/\tau_R) e^{-nE/k_B T}$ , where  $n$  is the number of neighbors of the particle before breaking,  $k_B$  is the Boltzmann constant,

and  $T$  is the temperature. By varying the attraction energy  $-E$  between neighboring particles, the SAK model permits a whole spectrum of fractal dimensions ranging from 1.35 to 2.0 in 2D, while in the Kolb model there is a unique fractal dimension of  $D = 1.57$  in 2D at dynamic equilibrium. It is worth noting that in the SAK model, there is also a dynamic equilibrium state where the cluster size no longer changes but the structure of clusters still changes with time, in contrast to the Kolb model, where the fractal dimension is fixed at  $D = 1.57$  in 2D at dynamic equilibrium. The other important result of the SAK model is that at a fixed time, the fractal dimension remains around 1.35 at large values of  $E$  and increases rapidly with decreasing  $E$  at about  $E \cong 4k_B T$ . The fractal dimension  $D \cong 1.35$  at large  $E$  is the result from the DLCA model in 2D and corresponds to the case  $E = \infty$  in the SAK model.

The experimental investigation was carried out by Liu *et al.*<sup>(15)</sup> using gold particles coated with a surfactant. With the use of static light scattering, conventional transmission electron microscopy (TEM), and high-resolution transmission electron microscopy (HRTEM), colloidal aggregates of small gold particles of approximately 15 nm in diameter were examined in great detail. The finite interparticle attractions were achieved with an appropriate additive, i.e., a surfactant, via adsorption. With the surfactant, particles within an aggregate were well separated at a distance of about 1–2 nm, about twice the width of the adsorbed surfactant layer, and infinite interparticle attraction at contact was avoided. With the modified Derjaguin–Landau–Verwey–Overbeek (DLVO) theory (see, e.g., ref. 16) to describe the interparticle interaction, it was shown that with the surfactant, the interparticle attraction energy becomes finite. Moreover, fractal aggregates can still be grown when the interparticle attraction is finite. The fractal dimension of the aggregates depends on the interparticle attraction energy: the minimum fractal dimension  $D$  that was obtained is about 1.74 for large interparticle attraction energies, with  $D$  increasing at smaller attraction energies. The experimental curve of  $D$  versus attraction energy resembles qualitatively that of the computer simulations of the SAK model,<sup>(14)</sup> although the simulations were done in 2D, indicating that the reversible aggregation process in a colloidal system is represented by the SAK model<sup>(14)</sup> rather than the Kolb model.<sup>(11)</sup>

## 2. COMPUTER SIMULATIONS

### 2.1. Model

The SAK model is a modification of the diffusion-limited-cluster-aggregation (DLCA) model. The computer simulations were done in a 2D

square lattice with periodic boundary conditions. The diffusion and the aggregation of particles and clusters in the SAK model are the same as in the DLCA model. The simulation starts with a given number of particles uniformly distributed on the lattice. Particles are performing Brownian motion (random walk). All particles and clusters move at random, one lattice constant in every time interval  $\tau_D$ . When two particles collide, they form a cluster. A cluster, just like a particle, then random walks as a unit and may collide with particles or clusters to form a larger cluster later. In the SAK model, the diffusion time constant for all clusters is assumed to be the same, since the cluster-size dependence of the diffusion time constant does not change the fractal dimension of the cluster.<sup>(8,17)</sup>

The major contribution of the SAK model is that it considers a *finite* nearest-neighbor interparticle interaction  $-E$  between particles, so that at finite temperatures, a particle within a cluster may break its bonds with its neighboring particles. At temperature  $T$ , the rate for a particle to unbind from its neighbors is  $(1/\tau_R) e^{-nE/k_B T}$ , where  $\tau_R$  is the time constant for unbinding, and  $n$  is the number of neighbors of the particle. For convenience, in this section, we will choose the units such that the Boltzmann constant is unity.

The unbinding time constant of a particle  $\tau_R$  may be different from the diffusion time constant  $\tau_D$ . The time constant  $\tau_R$  is the inverse of the unbinding attempt frequency and would depend more on the surface properties of the particles.  $\tau_D$  is related to the diffusivity of the particles in the solution. A large  $\tau_R/\tau_D$  may be interpreted as a higher particle mobility relative to relaxation and is analogous to the quenching rate in the glass transition. Approximately speaking, the Kolb model may be thought of as the case where  $\tau_R/\tau_D$  is very large. However, it should be noted that, as we have mentioned earlier, the SAK model differs from the Kolb model. In the Kolb model, the breaking unit is a bond which breaks at random, whereas in the SAK model the breaking unit is a particle which breaks its bonds with its neighbors according to the Boltzmann factor  $e^{-nE/T}$ .

The bond-breaking process is simulated with the Monte Carlo method. In every  $\tau_R$ , each particle is checked with a random number ranging from zero to unity. If the random number is larger than the Boltzmann factor  $e^{-nE/T}$ , the particle breaks all bonds with its neighbors. After the particle breaks the bonds with its neighbors, it then goes to one of the  $4-n$  unoccupied neighboring sites at random and the cluster is divided into segments. The resulting number of segments ranges from two to four, depending on the number of neighbors bonded to that particle and on the configuration of the cluster before the breakup. For example, the breaking away of a double-bonded particle in the neck portion of the cluster may result in as many as three segments, as illustrated in Fig. 1. Each individual

particle at question	unbinding rate	possible direction to move after unbinding	possible resulting configuration and resulting number of clusters	
①	$\frac{1}{\tau_R} e^{-E/T}$	N, E, S		  
②	$\frac{1}{\tau_R} e^{-2E/T}$	E, W		 
③	$\frac{1}{\tau_R} e^{-3E/T}$	N		

(a)

Fig. 1. Illustration of the unbinding processes of particles 1 through 3 in cluster (a). Unbinding takes place according to the rate  $(1/\tau_R) e^{-nE/T}$ , where  $n$  is the number of neighboring particles, and is simulated with the Monte Carlo method. The possible resulting configuration and possible number of resulting clusters, which is below the configuration, are shown for each case.

segment then becomes an independent cluster and may collide with others at a later time.

The bond breaking allows clusters to restructure and densify. One may regard the restructuring and densification in the SAK model as thermal annealing of the aggregates, since the bond-breaking processes are controlled by the Boltzmann factor. The DLCA model corresponds to the case when  $E$  is infinite and may be regarded as the quenched state.

In the simulations, only the translational motion of particles and clusters is considered explicitly and not the rotational motion. However, when there is sufficient sampling from the simulations to allow many configurations of two colliding clusters, rotational motion should not affect the fractal dimension of the clusters.<sup>(18)</sup>

**2.2. Results**

As examples, three different aggregation conditions with the same number densities but different values of  $E$  and  $\tau_R/\tau_D$  are shown in Figs. 2a-2c. Figure 2a shows the results when  $E=1.5T$  and  $\tau_R/\tau_D=0.2$ , in which large aggregates cannot easily be formed. Figure 2b shows the case

when  $E = 1.5T$  and  $\tau_R/\tau_D = 2$ , where aggregates are formed but quite a number of particles are still left in the fluid phase throughout the simulation. Figure 2c shows the case when  $E = 3.5T$  and  $\tau_R/\tau_D = 2$  in which almost no free particles remain in the solution and the cluster looks ramified. Figures 2a–2c together show the general trend of increasing cluster size with increasing  $E$  and  $\tau_R/\tau_D$ .

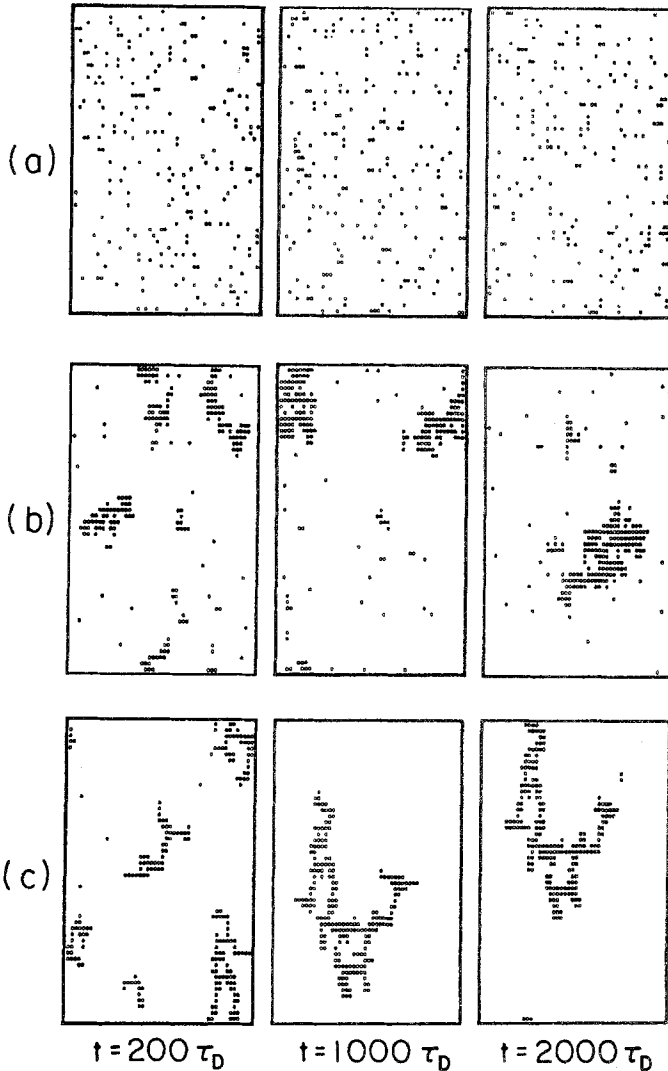


Fig. 2. Temporal evolution of various aggregation conditions with 212 particles on a  $50 \times 50$  square lattice: (a)  $E = 1.5T$  and  $\tau_R/\tau_D = 0.2$ , (b)  $E = 1.5T$  and  $\tau_R/\tau_D = 2$ , and (c)  $E = 3.5T$  and  $\tau_R/\tau_D = 2$ .

Two different procedures were used to investigate the effect of a finite attraction energy. Procedure 1 studies the restructuring effect by starting with clusters of various sizes  $N$  grown using the DLCA algorithm at the same particle number density and then activating the bond-breaking process according to the chosen values of  $E$  and  $\tau_R/\tau_D$ . This procedure is analogous to annealing. Under conditions of constant  $T$  and  $E$ , however, this procedure also represents cases where  $\tau_R/\tau_D$  is large. Under such conditions, aggregation occurs much faster than relaxation and the resultant aggregates initially resemble those of the DLCA model. Procedure 2 monitored the structural evolution of aggregates during growth. This was achieved by choosing smaller values of  $\tau_R/\tau_D$  so that sufficient unbinding took place along with cluster growth. It will be shown later that the results of the two procedures are quite similar.

For each set of  $E$  and  $\tau_R/\tau_D$ , the number of particles within a cluster  $N$  is plotted on a log-log scale against  $R_m$  in every  $100\tau_D$ , where  $R_m$  is the maximum radius of a cluster and is defined as

$$R_m = \frac{1}{2} \max_{\substack{1 \leq i, j \leq N \\ (i \neq j)}} \{|r_i - r_j|\} \tag{1}$$

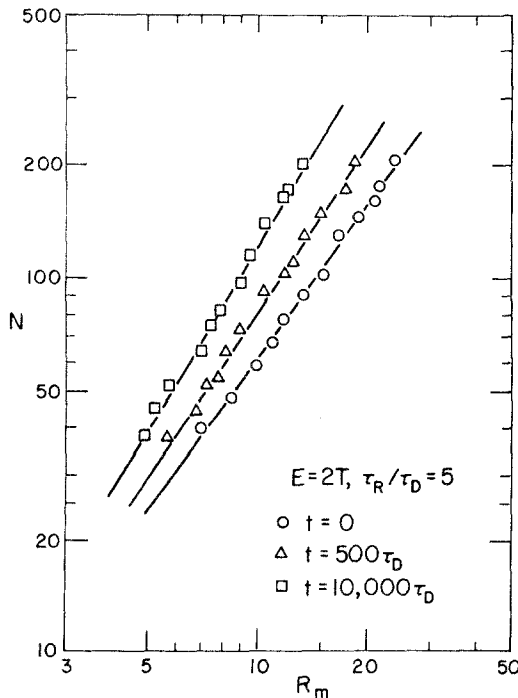


Fig. 3.  $N$  vs.  $R_m$ , where  $N$  is the cluster size and  $R_m$  is the maximum radius in units of the lattice constant as defined in the text.

In each plot of  $N$  versus  $R_m$ , 11–14 data points in the range  $30 \leq N \leq 200$ –300 are included; each point is the average over ten samples. The result is that the curves are linear throughout the simulation and the slope of the lines increases with time. An example done with procedure 1 is given in Fig. 3. Note that for a given  $N$ , the corresponding  $R_m$  decreases

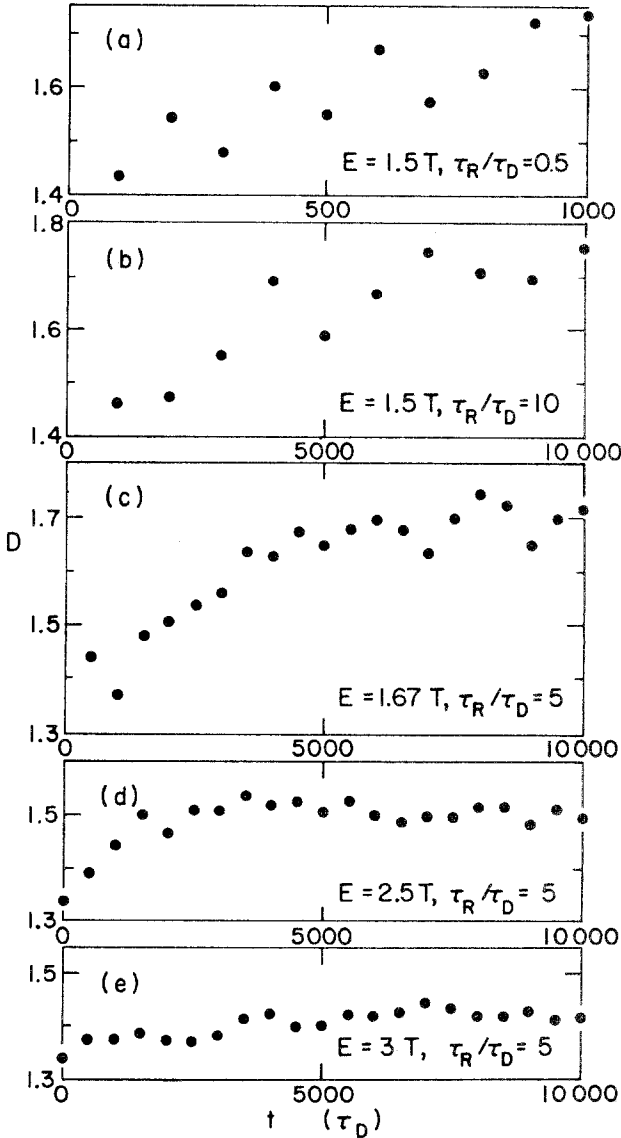


Fig. 4.  $D$  vs.  $t$  for various cases, where  $D$  is the fractal dimension and  $t$  is time.

with time, indicating that the clusters are getting denser with time. Meanwhile, the plots of  $t = 500\tau_D$  and  $t = 10,000\tau_D$  remain linear while the slope increases with time: 1.35 at  $t = 0$ , 1.46 at  $t = 500\tau_D$ , and 1.63 at  $t = 10,000\tau_D$ . This indicates that the clusters remain fractal during the course of restructuring and that the fractal dimension increases with time. The fractal dimension is taken as the slope of the  $\log N$  versus  $\log R_m$  lines by least-square fit. The plot of  $t = 0$ , which represents clusters grown from the DLCA model, thus has a fractal dimension  $D = 1.35 \pm 0.05$ , which agrees with the values obtained in refs. 8 and 9 within numerical error.

In Fig. 4,  $D$  versus  $t$  is plotted for various values of  $E$  and  $\tau_R/\tau_D$ . In Fig. 4a a small value,  $\tau_R/\tau_D = 0.5$ , was chosen and procedure 2 was used. Because of the small values of  $\tau_R/\tau_D$  and  $E$ , sufficient unbinding takes place along with cluster growth. In this case, when monitoring was stopped at  $t = 1,000\tau_D$ , the clusters were still growing. Thus, Fig. 4a can be regarded as the structural evolution of aggregates during growth and can be compared with Fig. 4b, which is obtained by using the same value for  $E$ , but a different value for  $\tau_R/\tau_D$  and procedure 1. The fluctuation of data points in both Figs. 4a and 4b is probably an artifact due to insufficient sampling. In spite of the different procedures used, the two curves look similar. The only difference is in the time scale. Thus, varying  $\tau_R/\tau_D$  only changes the time scale, but not the behavior of  $D$  versus  $t$ . With increasing  $E$ , the change in  $D$  becomes slower, as is shown in Figs. 4c-4e, obtained by procedure 1. Note that Figs. 4d and 4e both have the same value for  $D$ , 1.35 at  $t = 0$ , because the same initial clusters were used for comparison. In Figs. 4d and 4e,  $D$  quickly increases from the DLCA value and then saturates at some value  $D'$ , while  $D'$  decreases with increasing  $E$ :  $D' = 1.5$  for  $E = 2.5T$ ,  $D' = 1.42$  for  $E = 3T$ . This indicates that under suitable conditions aggregates can have a fractal dimension  $D$  that is substantially larger than the DLCA value;  $D$  remains unchanged over a long period of time, which has been observed experimentally.<sup>4,15</sup>

In Fig. 5,  $D$  versus  $E$  is plotted for  $\tau_R/\tau_D = 5$  at  $t = 5,000\tau_D$  and at  $t = 10,000\tau_D$  to show the different restructuring rates at different  $E$ . It is clearly shown that the change in  $D$  with time is accelerated when  $E$  is decreased from  $4T$ . Also note that for a given  $t$ ,  $D$  remains close to the DLCA value at large  $E$ , but drastically increases from that value at around  $E \leq 4T$ .

As we have shown in Fig. 4, the fractal dimension  $D$  changes with time and  $D$  may saturate for a long period of time. During the growth of clusters, the cluster size can also saturate. In general, the cluster size may saturate at a different time from the fractal dimension. In Fig. 6, to show the saturation of cluster size with time, we plotted the number of particles in the largest cluster  $N_m$  as a function of time for two cases,  $E = 1.67T$  (●)

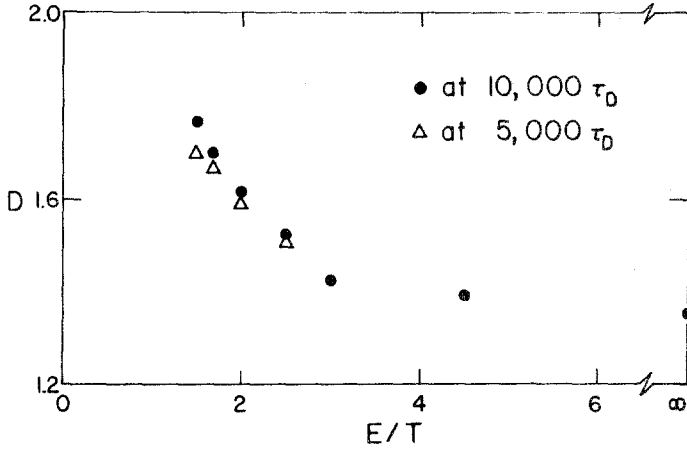


Fig. 5.  $D$  vs.  $E$  for  $\tau_R/\tau_D = 5$ , at (●)  $t = 10,000\tau_D$  and (Δ) at  $t = 10,000\tau_D$ .

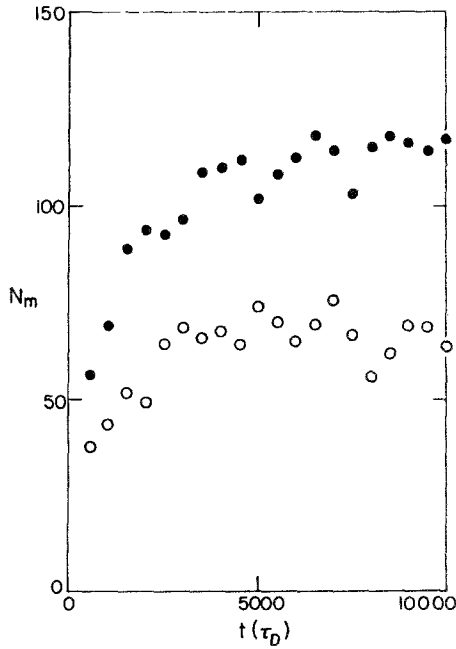


Fig. 6. The number of particles in the largest cluster  $N_m$  plotted as a function of time for two cases, (●)  $E = 1.67T$  and (○)  $E = 1.33T$ . For both cases,  $\rho = 0.11$  and  $\tau_R/\tau_D = 2$ , where  $\rho$  is the average particle number density.

and  $E = 1.33T$  ( $\circ$ ). For both cases,  $\rho = 0.11$  and  $\tau_R/\tau_D = 2$ , where  $\rho$  is the average particle number density. As one can see, in these two cases,  $N_m$  saturates very quickly. The saturation of  $N_m$  signals a pseudo-steady state in which the average number of particles within a cluster no longer changes, but the structure of the cluster is still changing. This pseudo-steady state corresponds to the dynamic equilibrium state in the Kolb model. The saturated  $N_m$  is a function of  $E$ , as shown in Fig. 7 for three different cases. The fact that the logarithm of the saturated  $N_m$  is linear with  $E$  for all cases indicates that the cluster size increases exponentially with  $E$ . The cluster size also increases with increasing  $\tau_R/\tau_D$  and particle concentration.

The behavior of the cluster size as a function of  $E$  can be understood qualitatively following the argument by Kolb.<sup>(11)</sup> Here we reproduce Kolb's argument with a modification on the breaking process. Let us suppose that the diffusion velocity  $v$  of a cluster of mass  $m$  is  $v = m^\alpha$  and, for simplicity, we also assume that the clusters have a uniform size. The time it takes for two clusters to pair up is then

$$t_a \sim \tau_D \frac{1}{\rho} \bar{m}^{-1} \propto (d \cdot 2)/D \tag{2}$$

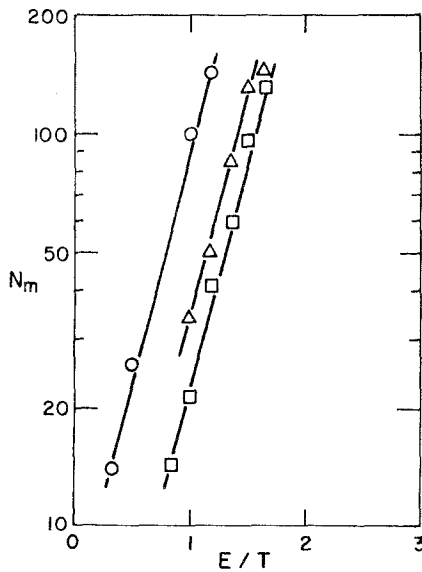


Fig. 7.  $N_m$  vs.  $E/T$ , where  $N_m$  denotes the number of particles in the largest cluster at ( $\circ$ )  $\rho = 0.051$ ,  $\tau_R/\tau_D = 5$ ; ( $\Delta$ )  $\rho = 0.125$ ,  $\tau_R/\tau_D = 2$ ; and ( $\square$ )  $\rho = 0.11$ ,  $\tau_R/\tau_D = 2$ ; where  $\rho$  denotes the number density.

where  $\bar{m} = N_0/N$  is the average mass per cluster,  $N$  is the total number of clusters,  $N_0$  is the total number of particles, and  $\rho = N_0/V$  is the average particle number density with  $V$  the volume of the system. The bond-breaking time  $t_f$  for a particle within a cluster of mass  $m$  is  $t_f \sim (\tau_R/m) e^{\bar{n}E/T}$ , where  $\bar{n}$  is the averaged number of neighbors of a particle within a cluster. The pseudo-steady state corresponds to  $t_a = t_f$ , which leads to

$$\bar{m} \sim \left( \frac{\rho \tau_R}{\tau_D} \right)^{1/[2 - \alpha - (d-2)/D]} e^{\bar{n}E/[2 - \alpha - (d-2)/D] T} \tag{3}$$

In the present study,  $\alpha = 0$  and  $d = 2$ ; thereby

$$\bar{m} \sim \left( \frac{\rho \tau_R}{\tau_D} \right)^{1/2} e^{\bar{n}E/2T} \tag{4}$$

The largest cluster size  $N_m$  can be related to the average cluster size  $\bar{m}$  by assuming an appropriate cluster size distribution function  $f(m)$ . A commonly used cluster size distribution is  $f(m) = A m^{-\tau} \exp(-m/N_m)$ , where  $A$  is some constant and we use  $N_m$  as the cutoff in the exponential tail. From the definition of  $\bar{m}$ ,

$$\bar{m} = \int_0^\infty f(m) m \, dm \tag{5}$$

we obtain  $\bar{m} = N_m^{2-\tau} \Gamma(2-\tau)$ , where  $\Gamma(2-\tau)$  is the gamma function with an argument  $2-\tau$ , which is independent of  $N_m$ . Therefore, we can expect

$$N_m \sim \left( \frac{\rho \tau_R}{\tau_D} \right)^{1/2} e^{\bar{n}E/[2(2-\tau) T]} \tag{6}$$

Preliminary results showed  $\tau \sim 1.5-2$ , depending on the value of  $\tau_R/\tau_D$ . The details of the kinetic studies will be published in a subsequent paper. However, the above argument provides a qualitative explanation for the exponential dependence of  $N_m$  on  $E$ .

### 3. GOLD PARTICLES WITH SURFACTANT

#### 3.1. Experiments

Colloidal gold particles were produced by reacting gold chloride with sodium citrate in an aqueous environment at 100°C.<sup>(19)</sup> The weight concentration of gold was about 0.0025% and that of sodium citrate was about 0.05%. The particles produced are roughly spherical, with a diameter of

about 15 nm. Aggregation of particles is induced by adding pyridine as in refs. 2, 4, and 5 or by adding different amounts of a surfactant at room temperature. The advantage, which will later become clear, of using a surfactant is that it keeps particles well separated.

Static light-scattering experiments were performed to obtain quantitative structural information, such as the fractal dimension  $D$  of the aggregates. The instrument, manufactured by Brookhaven Instrument Corporation, has a 50-mW helium–neon laser with wavelength  $\lambda = 632.8$  nm. For fractal aggregates, the scattering intensity of a given wave number  $q$  is related to the fractal dimension  $D$  in the form

$$I(q) \sim q^{-D} \quad (7)$$

over the range  $R_G^{-1} < q < a^{-1}$ , where  $a$  is the radius of the particles and  $R_G$  is the average radius of gyration of the aggregates.<sup>(20)</sup> Thus, the fractal dimension  $D$  of aggregates can be obtained by plotting  $I(q)$  versus  $q$  on double-logarithmic paper, where  $q$  is related to the scattering angle  $\theta$  by  $q = (4\pi n/\lambda) \sin(\theta/2)$ , and  $n$  is the refractive index of the fluid. The negative of the slope of the double-logarithmic plot of  $I(q)$  versus  $q$  in the power-law region gives the fractal dimension  $D$  of the aggregates.

Transmission electron microscopy (TEM) studies were carried out with a Philips EM 300 operated at 100 keV and were mainly used for direct visualization of the aggregates. In some cases, when the aggregates are more ramified (for example, when the fractal dimension  $D$  is smaller than 2.0) and particles do not overlap severely, the fractal dimension  $D$  of the aggregates can also be obtained by box counting.<sup>(20)</sup> The fractal dimension obtained from the TEM micrographs can be compared with that obtained from static light-scattering experiments. TEM samples were made by transferring a small amount of solution onto a carbon film suspended on a TEM copper grid.

In addition to static light-scattering experiments and conventional TEM studies, high-resolution transmission electron microscopy (HRTEM) studies were also carried out with a Philips 430T operated at 300 keV, which allowed the interparticle regions to be observed at the atomic length scale. The HRTEM studies permit the gain of *direct* knowledge about interparticle bonding, which is difficult to obtain otherwise.

### 3.2. Results

Various amounts of a cationic surfactant (Adgon 462, quaternary ammonium salt) are added to the initially dispersed suspension of gold particles of 15 nm diameter at room temperature to induce aggregation. This

surfactant is chosen because (i) it is soluble in water in a wide range of pH and (ii) it is positively charged, so that when it is adsorbed on the gold particle surface, it will neutralize the charges on the gold particles to induce aggregation. The initial negative charges on the particle surface are the result of adsorption of negatively-charged citrate during the growth process of gold particles.<sup>(21,22)</sup>

Figures 8a–8f are the TEM micrographs of gold particles with various surfactant concentrations  $c$ : (a)  $c = 0$ , (b)  $c = 1.87 \times 10^{-5}$  wt %, (c)  $4.67 \times 10^{-5}$  wt %, (d)  $9.33 \times 10^{-5}$  wt %, (e)  $3.73 \times 10^{-4}$  wt %, and (f)  $5.61 \times 10^{-4}$  wt %. One can see that with an increasing amount of surfactant, gold particles change from well dispersed, as in Fig. 8a, to aggregated, and the structure of the gold aggregates changes from dense to ramified as shown in Figs. 8a–8d, and back to dense again, as in Figs. 8e and 8f. The static light-scattering intensity of the aggregated samples corresponding to Figs. 8b–8e is shown in Fig. 9, where the double-logarithmic plots of  $I(q)$

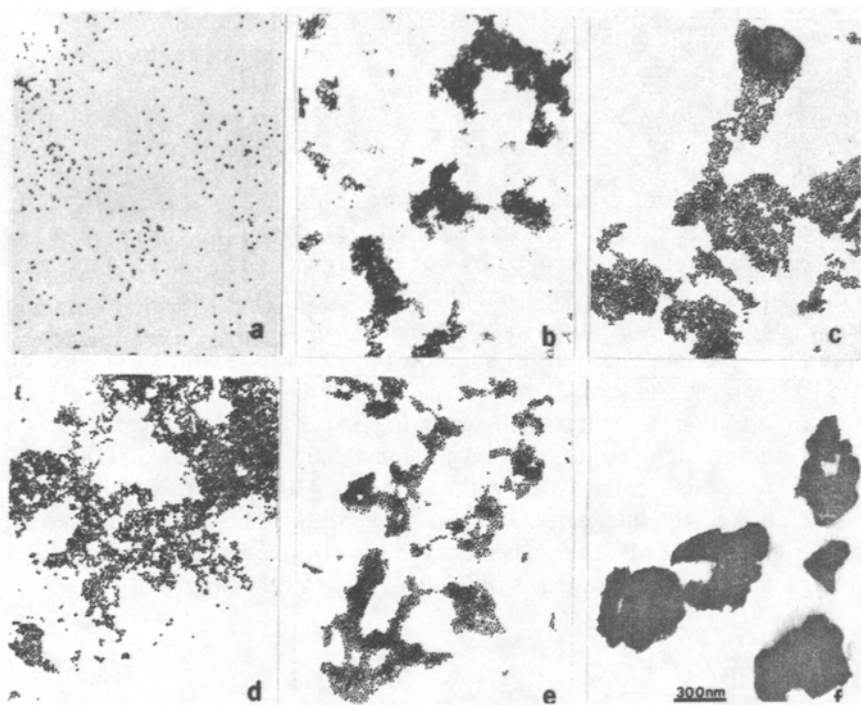


Fig. 8. TEM micrographs of gold particles at various surfactant concentrations  $c$ : (a)  $c = 0$ , (b)  $c = 1.87 \times 10^{-5}$  wt %, (c)  $4.67 \times 10^{-5}$  wt %, (d)  $9.33 \times 10^{-5}$  wt %, (e)  $3.73 \times 10^{-4}$  wt %, and (f)  $5.61 \times 10^{-4}$  wt %.

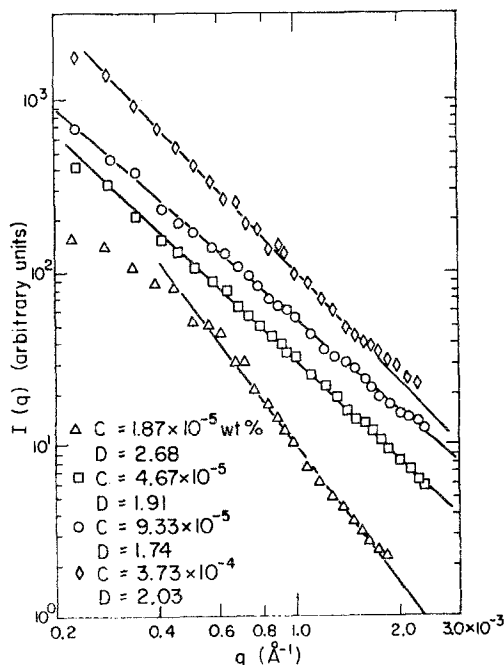


Fig. 9. Static light scattering intensity of the aggregated samples corresponding to ( $\Delta$ ) Fig. 8b,  $D = 2.68$ ; ( $\square$ ) Fig. 8c,  $D = 1.91$ ; ( $\circ$ ) Fig. 8d,  $D = 1.74$ ; ( $\diamond$ ) Fig. 8e,  $D = 2.03$ ; where  $D$  is the fractal dimension of the aggregates.

versus  $q$  clearly show a power-law behavior. The deduced values of the fractal dimension  $D$ , which are the negative of the slopes in Fig. 9, are as follows:  $D = 2.68$  for (b),  $D = 1.91$  for (c),  $D = 1.74$  for (d), and  $D = 2.03$  for (e). More detailed analysis of the data using the method proposed by Lin *et al.*<sup>(23)</sup> may yield additional information about the average radius of gyration. Here we are interested in the fractal dimension only. Both static light-scattering experiments and TEM micrographs indicate that the aggregates at  $c \geq 5.61 \times 10^{-4}$  wt % become compact objects. It is worth mentioning that for  $D \leq 2.0$ , the values of the fractal dimension obtained from static light scattering are identical to those obtained from box counting on TEM micrographs. For  $D > 2.0$ , particle overlapping prohibits accurate evaluation of  $D$  from TEM micrographs. The resultant fractal dimension  $D$  as a function of the added surfactant concentration  $c$  is shown in Fig. 10. The value of  $D$  decreases as the surfactant concentration  $c$  is increased and reaches the minimum value 1.74 at  $c = 9.33 \times 10^{-5}$  wt %, above which the value of  $D$  increases again.

The role of the surfactant is to change the interparticle interaction via adsorption. The adsorption of the surfactant on the gold particle surface is

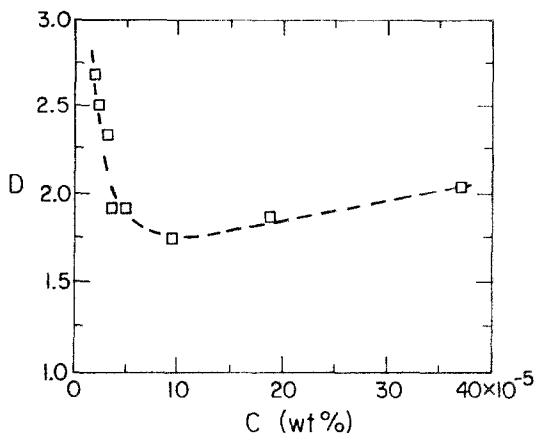


Fig. 10.  $D$  vs.  $c$ , where  $D$  is the fractal dimension and  $c$  is the surfactant concentration.

evident by the onset of the aggregation of the gold particles in our experiment. This point will become clear later when the interparticle interaction is shown quantitatively. More detailed adsorption studies of similar surfactants have been done on colloidal silver surfaces.<sup>(24,25)</sup> The adsorption behavior of the surfactant used in this experiment on gold particle surfaces should be similar to that described in refs. 24 and 25 because of the colloidal similarity. Initially, the adsorbed surfactant ions on the gold particle surface help reduce the surface charge of the particles and, hence, increase the net interparticle attraction. This is due to the initial opposite charge of the surfactant ions and the gold surface. When the surface charge on the gold particles is completely neutralized, the net interparticle attraction reaches a maximum; further adsorption of the surfactant only increases the surface charge of the gold particles, which now have an opposite sign, and thus reduces the net interparticle attraction. The observed minimum fractal dimension at  $c = 9.33 \times 10^{-5}$  wt % corresponds to the maximum in the interparticle attraction. The minimum  $D$  value of 1.74 obtained at  $c = 9.33 \times 10^{-5}$  wt % is quite reasonable, for it agrees with both the computer simulations of the irreversible diffusion-limited-cluster-aggregation (DLCA) model corresponding to the case of an infinite interparticle attraction and the previous aggregation studies of gold particles with pyridine addition in the fast aggregation regime.<sup>(2,4)</sup>

The difference in using a surfactant instead of pyridine to modify the interparticle interactions is revealed in the HRTEM micrographs in Figs. 11a and 11b, where gold aggregates with the surfactant and with pyridine are shown, respectively. With the surfactant, the gold particles remain well separated at a distance of about 1–2 nm, which is about twice

the width of the adsorbed surfactant layer,<sup>(26,27)</sup> as evidenced by the clear gaps between gold particles in Fig. 11a. In contrast, with the addition of pyridine, necks form between adjacent gold particles as shown in Fig. 11b. This may explain why in the previous aggregation studies of gold particles with pyridine, change in the structure of aggregates has seldom been observed and only certain values of the fractal dimension have been obtained, i.e., 1.75 for fast aggregation and 2.0 for slow aggregation. From Fig. 11b, one can see that it is very difficult to break the necks once they form. Consequently, with pyridine, rearrangement of particles within a cluster is almost impossible.

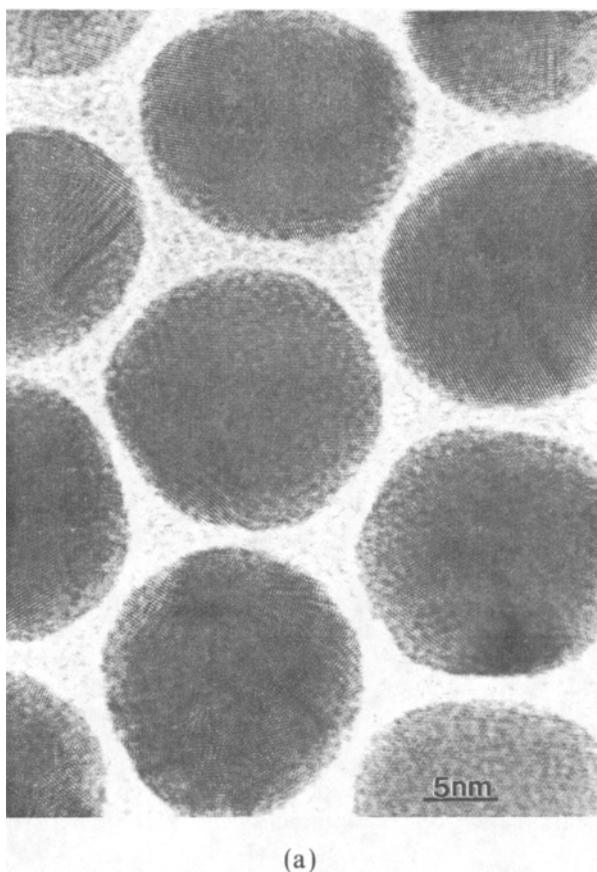


Fig. 11. HRTEM micrographs of gold aggregates (a) with the surfactant and (b) with pyridine. Gold particles are well separated at a distance of 1–2 nm with the surfactant, while necks form between particles with pyridine.

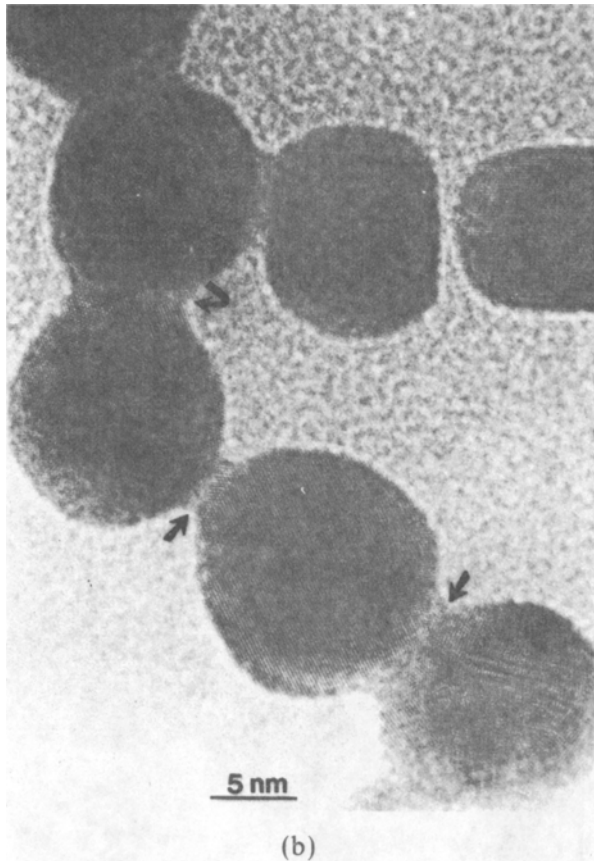


Fig. 11. (Continued)

The use of the surfactant allows the gold particles to remain well separated even at the closest distance, i.e., twice the length of the adsorbed surfactant layer. It is therefore possible to talk about the interaction between gold particles in the case of surfactant addition. Since the experiments are done in very dilute suspensions and the particles remain separated even at the closest approach of about 1–2 nm, it is adequate to describe the interparticle interaction with a modified DLVO theory. Under the electrostatic condition, the interaction between gold particles  $V(s)$  has two terms:

$$V(s) = V_c(s) + V_a(s) \quad (8)$$

where  $V_c(s)$  is the screened Coulomb interaction, with the Debye–Hückel approximation, which is justified under the present experimental conditions

where both the particle and electrolyte concentrations are low,  $V_a(s)$  is the van der Waals attraction, and  $s$  is the surface-to-surface interparticle distance. In CGS units,  $V_c(s)$  takes the form<sup>(13)</sup>

$$V_c(s) = \frac{Z^2 e^2}{\epsilon r} \left[ \frac{e^{qa}}{1 + qa} \right]^2 e^{-qr} \quad (9)$$

where  $a$  is the radius of a particle,  $r = s + 2a$  is the separation between the centers of particles,  $Z$  is the surface charge of a particle,  $\epsilon$  is the static dielectric constant of water,  $e$  is the electronic charge, and  $q$  is the inverse screening length, which satisfies

$$q^2 = \frac{4\pi e^2}{\epsilon k_B T} \sum_i n_i z_i^2 \quad (10)$$

where  $k_B$  is the Boltzmann constant,  $T$  is the absolute temperature, and  $z_i$  and  $n_i$  are the charge and the number density of the  $i$ th species of ions, respectively. The term in brackets in Eq. (9) is the size correction, which takes into account the fact that part of the volume of the suspension is not available for screening due to the finite size of the colloidal particles.

The van der Waals attraction takes the following form in CGS units:<sup>(16)</sup>

$$V_a(s) = \frac{A}{6} \left[ \frac{2a^2}{s^2 + 4as} + \frac{2a^2}{s^2 + 4as + 4a^2} + \ln \left( \frac{s^2 + 4as}{s^2 + 4as + 4a^2} \right) \right] \quad (11)$$

where  $A$  is the Hamaker constant.

To calculate the interparticle interaction, a Hamaker constant of  $2.2 \times 10^{-12}$  erg is used, which is typical of metals.<sup>(28)</sup> For the screening length  $q^{-1}$ , the contributions from all ions in the solution are included; the pH is about 5. The number concentrations of  $\text{Cl}^-$ ,  $\text{Na}^+$ , and citrate are about  $1.56 \times 10^{16} \text{ cm}^{-3}$ ,  $1.74 \times 10^{18} \text{ cm}^{-3}$ , and  $0.58 \times 10^{18} \text{ cm}^{-3}$ , respectively. The surfactant concentration is on the order of  $10^{-5}$  wt %. The dominant contribution is from  $\text{Na}^+$  ions. Using Eq. (9), a value of about 7 nm is obtained for the screening length  $l = q^{-1}$ . For the effective surface charge  $Z$  of a particle, the electrical mobility of the particle  $\mu$  has been measured to be  $4.83 \times 10^{-4} \text{ cm}^2/\text{V sec}$  in the absence of the surfactant. From the electrical mobility measurement, the  $\zeta$  potential of the particles is deduced to be about 100 mV. By approximating the  $\zeta$  potential  $V_\zeta$  in the CGS units to be

$$V_\zeta = \frac{Ze^2}{\epsilon a} \quad (12)$$

the charge  $Z$  of each particle is estimated to be about 42 times the electron charge in the absence of surfactant ions. It should be noted that this effective charge  $Z$  may differ from the real surface charge. However, it is the effective charge  $Z$  that determines the electrostatic repulsion between particles. The surface charge  $Z$  is taken to be 0 at the surfactant concentration  $c = 9.33 \times 10^{-5}$  wt % where the fractal dimension  $D = 1.74$  is the minimum. When complete adsorption of surfactant molecules is assumed, the surface charge of particles at a given surfactant concentration  $c$  can then be linearly interpolated in the range  $0 < c < 9.33 \times 10^{-5}$  wt %. By complete adsorption, we mean that all the added surfactant ions are on the gold particle surfaces. For example, the interpolated values of the effective surface charge  $Z$  are 34 for  $c = 1.87 \times 10^{-5}$  wt % (Fig. 8b), and  $Z = 21$  for  $c = 4.67 \times 10^{-5}$  wt % (Fig. 8c), respectively. The value of  $Z$  for  $c > 9.33 \times 10^{-5}$  wt % was not extrapolated. The asymmetry of  $D$  versus  $c$  near the minimum in Fig. 11 indicates that the assumption of complete adsorption of surfactant is no longer valid for  $c > 9.33 \times 10^{-5}$  wt %.

Using the estimated values of  $Z$ ,  $q$ ,  $A$ , etc., the interparticle interaction  $V(s)$  was then calculated for the surfactant concentration range  $0 < c < 9.33 \times 10^{-5}$  wt %. The result is shown in Fig. 12. The closest separation between two particles, which is about twice the length of an adsorbed surfactant molecule (1.5 nm), is indicated by the dashed line at  $s = 1.5$  nm, which is a reasonable value when the structure and the configuration of the

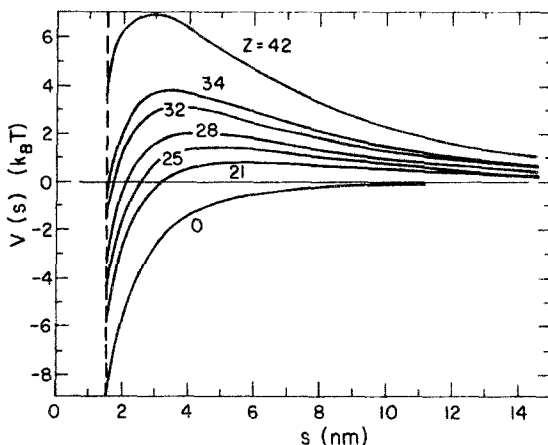


Fig. 12.  $V(s)$  vs.  $s$  for various values of the effective surface charge  $Z$  of gold particles, where  $V(s)$  is the interparticle interaction energy in units of  $k_B T$  and  $s$  is surface-to-surface interparticle distance. The dashed line at  $s = 1.5$  nm indicates the closest interparticle separation due to surfactant adsorption. The different values of  $Z$  are the result of different adsorption amounts of surfactant ions on the gold particle surface.

absorbed surfactant are considered.<sup>(25,26)</sup> It was approximated that the contribution of the steric repulsion between two adsorbed surfactant layers to the interparticle interaction is a hard-wall repulsion at the average separation  $s = 1.5$  nm. As the surfactant concentration  $c$  is increased, one can see that the interaction at  $s = 1.5$  nm changes from repulsive to attractive at about  $c = 1.87 \times 10^{-5}$  wt %, which agrees very well with the onset of aggregation in the experiment. As the surfactant concentration  $c$  is further increased, the net attraction at  $s = 1.5$  nm becomes larger, which is consistent with the decrease in the fractal dimension shown in Fig. 10.

As mentioned above, the onset of aggregation of the gold particles serves as evidence of the adsorption of the surfactant on the particle surface. The reason is as follows. If the surfactant ions do not adsorb on the gold particle surface, but remain in the suspension, given the low surfactant concentrations that are used, mere screening by the free surfactant ions in the suspension would not reduce the Coulomb repulsion between gold particles enough to induce aggregation.

The value of  $|V(s)|$  at  $s = 1.5$  nm is the maximum attraction energy that two particles can experience, since they cannot get any closer. In Fig. 13, the fractal dimension  $D$  is plotted as a function of the absolute value of the net attraction at  $s = 1.5$  nm,  $|V_{1.5\text{nm}}|$ , for the aggregated cases in the range  $0 < c < 9.33 \times 10^{-5}$  wt %. First, one sees that with the addition of the surfactant, the interparticle attraction energy now remains finite. Second, with finite interparticle attraction energies, the gold particles still

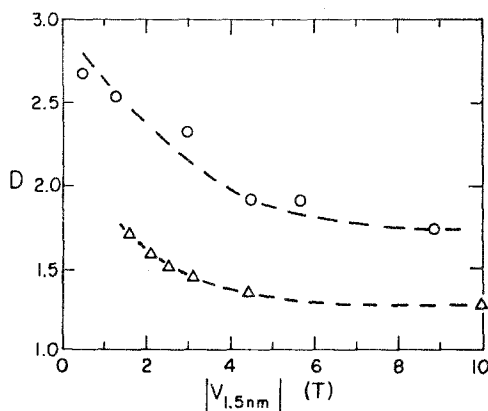


Fig. 13.  $D$  vs.  $|V_{1.5\text{nm}}|$  for the aggregated samples ( $\circ$ ), where  $D$  is the fractal dimension and  $|V_{1.5\text{nm}}|$  is the net interparticle attraction energy at  $s = 1.5$  nm. Also plotted (dashed line) is  $D$  vs.  $|E|$  from the computer simulations of ref. 12 ( $\triangle$ ), where  $|E|$  is the nearest-neighbor attraction energy in ref. 12. Both  $|V_{1.5\text{nm}}|$  and  $|E|$  are in units of  $T$ . The Boltzmann constant is taken to be unity here.

form fractal aggregates. The fractal dimension remains around 1.74 at large values of  $|V_{1.5\text{nm}}|$  and increases as  $|V_{1.5\text{nm}}|$  decreases. Also plotted in Fig. 13 is the curve for  $D$  versus  $E$  of the computer simulations of the SAK model shown in Fig. 8 at  $t = 10,000\tau_D$ . Note the similarity of the two curves, although the simulations were done in 2D: the values of the fractal dimension  $D$  in both curves remain constant for large values of the attraction energy and increase when the attraction energy is about  $4T$ , where  $T$  is the absolute room temperature in the experimental case. The Boltzmann constant is taken to be unity here. The close resemblance between the two curves and the saturation of  $D$  at  $E \sim 4T$  suggest that the reversible aggregation process in a colloidal system is represented by the SAK model. While effects of the structural change have been studied by other investigators, none of these studies can explain the observed *continuous* change of the fractal dimension with interparticle interactions. For example, random bond breaking only increases the fractal dimension from 1.75 to 2.03 in 3D.<sup>(11)</sup> The RLCA model gives a fractal dimension  $D = 2.0$  in 3D.<sup>(10)</sup> The rotational adjustment of one cluster around the center of another cluster at collision to allow a second bond to form only increases the fractal dimension slightly in 2D<sup>(29)</sup> and by about 0.3 in 3D.<sup>(30)</sup>

The choice of the attraction energy at  $s = 1.5$  nm may appear somewhat arbitrary, since the interparticle separation in the HRTEM micrographs ranges from 1–2 nm. However, the conclusion drawn from Fig. 13 would not be altered if the interaction energy at a different value of  $s$  is chosen. For instance, the interaction at  $s = 1$  nm or 2 nm could have been used instead, which would only change the specific values of the interaction energy, but not the qualitative behavior of the fractal dimension versus the interaction energy.

#### 4. SUMMARY

Aggregation of colloidal particles with a *finite* interparticle attraction energy has been investigated with computer simulations and with colloidal gold particles. The computer simulations were done with the SAK model, which incorporates a finite nearest-neighbor attraction energy  $-E$  into the DLCA model. Experiments were done with gold particles coated with a surfactant. The adsorbed surfactant layer modified the interparticle interaction in two ways: (1) the adsorbed layer kept two particles separated, preventing the infinite attraction at contact; and (2) the charge of the adsorbed surfactant modified the interparticle interaction at finite distances. The interparticle interaction can be well described by the modified DLVO theory. Both the computer simulations of the SAK model and the experiments showed that (i) with a finite interparticle attraction energy,

aggregates can remain fractal, and (ii) the fractal dimension remains that of the DLCA model at large attraction energies and increases rapidly at small attraction energies. The agreement between the computer simulations of the SAK model and the experimental results of gold aggregates suggests that the reversible aggregation process in a colloidal system can be represented by the SAK model.

In the computer simulations, the fractal dimension can also change with time:  $D$  may change with time continuously or saturate at some value for a long period of time, depending on the interparticle attraction energy and the ratio of two time constants, i.e., the diffusional time constant  $\tau_D$  and the relaxational time constant for bond breaking  $\tau_R$ . In the experimental study, the change of  $D$  with time was not observed. It could be that the present system represents the case where  $\tau_R/\tau_D$  is large and the fractal dimension  $D$  is saturated at some value for a long time. However, in a separate study of the growth of colloidal gold particles, Liu *et al.* did observe the change of  $D$  with time.<sup>(31)</sup>

## ACKNOWLEDGMENTS

This work was supported by the Air Force Office of Scientific Research (AFOSR) and Department of Advanced Research Projects Agency (DARPA) and monitored under grant no. AFOSR 87-0114 and 91-0040.

## REFERENCES

1. T. A. Witten and L. M. Sander, *Phys. Rev. Lett.* **47**:1400 (1981).
2. D. A. Weitz and M. Olivera, *Phys. Rev. Lett.* **52**:1433 (1984).
3. C. Aubert and D. S. Cannell, *Phys. Rev. Lett.* **56**:738 (1986).
4. P. Dimon, S. K. Sinha, D. A. Weitz, C. R. Safinya, G. S. Smith, W. A. Varady, and H. M. Lindsay, *Phys. Rev. Lett.* **57**:595 (1986).
5. D. A. Weitz, J. S. Huang, M. Y. Liu, and J. Sung, *Phys. Rev. Lett.* **54**:1416 (1985).
6. D. A. Schaefer, J. E. Martin, P. Wiltzius, and D. S. Cannell, *Phys. Rev. Lett.* **52**:2371 (1984).
7. J. C. Parity and P. M. Pusey, in *On Growth and Form*, H. E. Stanley and N. Ostrowsky, eds. (Nijhoff, Dordrecht, 1986), p. 219.
8. P. Meakin, *Phys. Rev. Lett.* **51**:1119 (1983).
9. M. Kolb, R. Botet, and R. Jullien, *Phys. Rev. Lett.* **51**:1123 (1983).
10. M. Kolb and R. Jullien, *J. Phys. Lett. (Paris)* **45**:L977 (1984).
11. M. Kolb, *Phys. Rev. Lett.* **53**:1653 (1984).
12. A. T. Skjeltorp, *Phys. Rev. Lett.* **58**:1444 (1987).
13. W. Y. Shih, I. A. Aksay, and R. Kikuchi, *J. Chem. Phys.* **86**:5127 (1987); and references therein.
14. W. Y. Shih, I. A. Aksay, and R. Kikuchi, *Phys. Rev. A* **36**:5015 (1987).
15. J. Liu, W. Y. Shih, M. Sarikaya, and I. A. Aksay, *Phys. Rev. A* **41**:3206 (1990).
16. J. Th. G. Overbeek, *J. Colloid Interface Sci.* **58**:408 (1977).

17. P. Meakin, in *On Growth and Form*, H. E. Stanley and N. Ostrowsky, eds. (Nijhoff, Dordrecht, 1986), p. 111.
18. P. Meakin, *Phys. Rev. A* **27**:604 (1983).
19. J. Turkevich, P. C. Stevenson, and J. Hillier, *Trans. Faraday Soc. Disc.* **11**:55 (1951).
20. J. Teixeira, in *On Growth and Form*, H. E. Stanley and N. Ostrowsky, eds. (Nijhoff, Dordrecht, 1986), p. 145.
21. O. Siiman, L. A. Bunm, R. Callaghan, C. G. Blatchford, and M. Kerker, *J. Phys. Chem.* **87**:1014 (1983).
22. J. P. Jolivet, M. Gzara, J. Mazieres, and J. Lefebvre, *J. Colloid Interface Sci.* **107**:429 (1985).
23. M. Y. Lin, H. M. Lindsay, D. A. Weitz, R. C. Ball, R. Klein, and P. Meakin, *Phys. Rev. A* **41**:2005 (1990).
24. R. H. Ottewill and M. C. Roastogi, *Trans. Faraday Soc.* **56**:866 (1960).
25. K. Osseo-Asare, D. W. Fuerstenau, and R. H. Ottewill, in *American Chemical Society Symposium*, No. 8 (ACS, Washington, D. C., 1978), p. 63.
26. R. H. Ottewill and A. Watanabe, *Kolloid-Z.* **170**:132 (1960).
27. M. J. Rosen, *Surfactants and Interfacial Phenomena* (Wiley, New York, 1978), p. 67.
28. D. J. Shaw, *Introduction to Colloidal and Surface Science* (Butterworth, Boston, 1980), p. 190.
29. P. Meakin and R. Jullien, *J. Phys. (Paris)* **46**:1543 (1985).
30. P. Meakin and R. Jullien, *J. Chem. Phys.* **89**:246 (1985).
31. J. Liu, Ph.D. Thesis, University of Washington (1990).